

A CONTINENTAL SCALE VEGETATION INDEX FROM INDIAN GEOSTATIONARY SATELLITE

Rahul Nigama*, Bimal K. Bhattacharyaa, Keshav R. Gunjala, N. Padmanabhanb and N.K. Patela

^aAgriculture-Forestry and Environment Group, (RESA) Space Applications Centre (ISRO)
Ahmedabad 380 015, India – (rahulnigam, bkbhattacharya, keshavgunjal, nkpatel)@sac.isro.gov.in

^bData Products Software Group, (SIPA) Space Applications Centre (ISRO)
Ahmedabad 380 015, India – sacpaddy@sac.isro.gov.in

KEYWORDS: NDVI, Geostationary, CCD, INSAT, Asia

ABSTRACT:

Time series vegetation index is a valuable source to derive several plant biophysical parameters, land use land cover change dynamics and to study climatic behavior. Geostationary satellite sensor is capable of observing earth surface with continental coverage in a single snapshot at constant viewing direction with high temporal frequency (half-an-hour). INSAT 3A CCD is the only geostationary sensor to acquire regular coverage of Asia continent at 1 kmX1km spatial resolution. A retrieval algorithm of surface reflectances in red, near infrared (NIR), short wave infrared (SWIR) and NDVI from INSAT 3A CCD has been defined and integrated in the operational chain. This includes (i) vicarious calibration with IRS P6 AWiFS bands (ii) cloud screening based on band thresholds and atmospheric correction of at-sensor reflectances using SMAC (Simple Model for Atmospheric correction) models. The atmospheric correction improved the NDVI by 5-40% and also increased its range. The temporal dynamics of 16-day NDVI composite at 0500 GMT for a growing year (June 2008-April 2009) showed matching profiles with reference to global products (MODIS TERRA) over known land targets such as agriculture, forest and desert. The root mean square deviation (RMSD) between the two was 0.13 with correlation coefficient (r) 0.8 from 270 paired datasets. This cross-correlation would help in NDVI calibration to add continuity in long term NDVI database for climate change studies.

1. INTRODUCTION

The vegetation indices are derived by combining spectral data in different wave bands. The spectral indices are typically a sum, difference, ratio or other linear combinations of reflectance factor or radiance observation from two or more wavelength intervals (Wiegand et al., 1991). Vegetation indices show better sensitivity than individual spectral bands for the detection of biomass (Asrar et al., 1984). Vegetation indices have been used for evaluation of vegetation crop density, crop discrimination and crop prediction (Bannari et al., 1995). Generally spectral data in red and near infrared bands are used for development of vegetation indices. These vegetation indices have been found useful for vegetation density (Wiegand et al., 1979; Spanner et al., 1990), green leaf density, photosynthesis active biomass (Tucker, 1979; Wiegand et al., 1991) absorbed photosynthetically active radiation and evapotranspiration. Bannari et al., (1995) has listed over forty vegetation indices developed in the area of applications and research in satellite remote sensing.

The “Normalized Difference Vegetation Index” (NDVI) is widely used for vegetation growth monitoring. NDVI was originally used as a measure of green biomass (Tucker *et al.*, 1986). It has a strong theoretical basis as a measure of the solar photosynthetic active radiation absorbed by the canopy (Sellers, 1985). The spectral characteristics of vegetation show that reflectances in green (550nm) and red band (650nm) are mainly pigment (e.g. chlorophyll) controlled. The reflectances in near infrared band (around 800nm) are controlled by total internal reflection due to gradients in refractive index due to leaf mesophyll tissue. The NDVI relates reflectance (or radiance) in the red range and in the

NIR range to vegetation variables such as leaf area index (LAI), canopy cover, and the concentration of the total chlorophyll. It is sensitive to low chlorophyll contents, to low fraction of vegetation cover and, as a result, to low level of absorbed photosynthetic active solar radiation. But it is not sensitive at higher chlorophyll contents or to rate of photosynthesis for large vegetation coverage. For land surfaces dominated by vegetation, the NDVI values normally range from 0.1 to 0.8 during the growth season, the higher values being associated with greater density and greenness of the plant canopy. Atmospheric effects, such as Rayleigh scattering from molecules, Mie scattering by aerosols, gaseous absorption by atmospheric constituents and sub-pixel-sized clouds, all tend to increase the value of red with respect to NIR and reduce the values of the computed vegetation indices. The quantitative estimation of most of the biophysical parameters using satellite based optical remote sensing requires time series NDVI data as model inputs. Daily and time composited NDVI series from moderate (1km) to coarse (>1km) resolution sensor data can provide ‘full resolution’ of vegetation growth cycle than a single date high resolution optical data with low repeativity.

The normalized difference vegetation index (NDVI) product is now-a-days regularly available from observations in red and near infrared bands in large – view global polar orbiting sensors such as: SPOT-VGT, MODIS TERRA and AQUA, NOAA AVHRR at spatial resolutions varying from 250m to 8km. These are available maximum twice per day on daily or time composite basis. The NDVI generated at multiple times in a day from geostationary satellite sensors provide opportunity to get more cloud free NDVI as compared to once or twice overpasses in a day by polar orbiting large view sensor (Fensholt *et al.*, 2006). The effects due to orbital

drift as in NOAA AVHRR will be least because of constant viewing geometry of geostationary sensors with respect to earth targets. Moreover, the diurnal behaviour of narrow band surface reflectances is ideal to study BRDF characteristics of similar homogeneous land targets having similar sensor viewing conditions. This again helps further correct NDVI through surface BRDF modeling. No other existing geostationary satellite missions in the world except INSAT 3A CCD (1km) of India and Feng Yung of China and MSG SEVIRI (3 km) have payloads that take multiple observations per day in narrow spectral optical bands (red, NIR and SWIR) at 1km X 1km spatial resolution. INSAT 3A has CCD payload was specifically designed to monitor vegetation and snow cover conditions over Asian region regularly. The present study was undertaken with the following objectives:

- (i) To define algorithm theoretical basis document (ATBD) for NDVI from INSAT 3A CCD narrow band optical data.
- (ii) To integrate the NDVI algorithm in the automated processing chain and validate the operational products

2. METHODOLOGY

The reflected radiances from earth surface reaching satellite sensors are generally influenced by sun-sensor viewing geometry and atmospheric noises, adjacency and BRDF (Bi-directional Reflectance Distribution Function) effects. Corrections are needed to remove these effects to convert spectral reflectances (R_i) at sensor into surface spectral reflectances. These corrections are categorized as:

Level 1: Generation of angular normalized atmospherically corrected surface spectral reflectances

Level 2: Level 1 + adjacency effect correction

Level 3: Level 2 + BRDF correction

Level 1 correction has three different components

A. Rayleigh scattering

B. Gaseous absorption (ozone, water vapour, CO₂)

C. Aerosol scattering and absorption

2.1 Post-launch vicarious calibration of band radiances

It has been found from earlier analysis that NDVI computed with pre-launch calibration coefficients for red and near infrared (NIR) bands showed significant non-linear bias that increased with increase in NDVI values (Bhattacharya *et al*, 2008). Further studies also found that radiance in NIR band at TOA become saturated for higher values of radiance during pre-launch calibration. The electronic performance of CCD sensor elements generally is degraded due to space weathering. Direct calibration with *in situ* ground measurements is also not feasible for such coarser spatial resolution (1km) due to lack of homogeneous patch and spatial representativeness of ground measurements. Therefore, a cross-calibration has been carried out with collocated, coregistered and calibrated TOA radiances of red and NIR bands of similar spectral response from high resolution (56 m) IRS-P6 AWiFS sensor with equal atmospheric perturbations. Three clear sky dates spread over December (2007), February (2008) and March (2008) for both INSAT 3A CCD and AWiFS having same overpass time (0500 GMT) were chosen for cross-calibration. TOA band radiances from

six different land covers such as: agriculture, forest, snow, bare soil, water body and cloud were used for recalibration.

2.2 Cloud screening

The optical properties of clouds showed that its reflectances in red, NIR or cloud albedo in broad visible band become high and even more than 90%. But SWIR band reflectances are less in presence of water clouds due to higher absorption. Three criteria were fixed for cirrus (high level), alto (medium level) and cumulus (low level) clouds based on several CCD scenes. The first two criteria are only based on TOA reflectance thresholds in red and NIR bands due to presence of more of ice cloud. In third criteria, SWIR TOA reflectance threshold was introduced in addition to red and NIR reflectances due to increasing presence of water clouds. Further processing was carried out only in cloud free pixels.

2.3 Atmospheric correction

The TOA reflectances in cloud free pixels were corrected for atmospheric noises such as molecular (Rayleigh) and aerosol (Mie) scattering along with gaseous absorption using simple model for atmospheric correction (SMAC) with default coefficients (Rahman and Dedieu, 1994). That has been successfully used for large view satellite sensors such as NOAA AVHRR, METEOSAT etc. The generalized functional form of SMAC model is

$$\rho(\theta_s, \theta_v, \Delta\phi) = t_g(\theta_s, \theta_v) \left\{ \rho_a(\theta_s, \theta_v, \Delta\phi) + [e^{-\tau/\mu_s} + td(\theta_s)] \frac{[\rho_c e^{-\tau/\mu_v} + \rho_e td(\theta_v)]}{1 - \rho_e S} \right\}$$

μ_s = cosine of the Sun zenith angle

μ_v = cosine of the viewing zenith angle

$\Delta\phi$ = relative azimuth between Sun and satellite direction

t_g = total gaseous transmission

ρ_a = Atmospheric reflectance which is a function of molecule and aerosols optical properties, illumination angle, viewing angle and relative azimuth between Sun and the observer

τ = atmospheric optical depth ($e^{-\tau/\mu_s}$ and $e^{-\tau/\mu_v}$ being the direct atmospheric transmission)

$td(\theta_s), td(\theta_v)$ = atmospheric diffuse transmittances

S = Spherical albedo of the atmosphere

$1 - \rho_e S$ = taken in account multiple scattering

between surface and the atmosphere

This includes 1st order correction for additive and multiplicative atmospheric perturbations and assume surface is lambertian. Moreover, this scheme is simple to implement, calibrated and tested against 5S atmospheric radiative transfer code and is thus increasingly used for generating surface reflectances from TOA radiances. Apart from sun-sensor angular geometry, this requires atmospheric inputs such as columnar ozone, precipitable water and

aerosol optical depth (AOD) at 0.55 μm . The database on daytime mean of five years' (2002 – 2006) ozone, precipitable water and aerosol optical depth at 0.55 μm from MODIS TERRA (0530 GMT) and AQUA (0800 GMT) was prepared through interpolation of MODIS eight-day atmospheric products ($1^\circ 1^\circ$) equivalent to CCD resolution. These were further used as inputs to SMAC to compute surface reflectances.

2.4. NDVI product formatting

The computation of NDVI was carried out in cloud free pixels using surface reflectances in CCD red and NIR bands. The NDVI was scaled to binary (8-bit) format with offset = 110 and gain = 0.01. The end product contains NDVI in h5 format that contains cloud free NDVI, surface band reflectances as well as files for angular geometry for the geographical bound ($44.5^\circ - 105.3^\circ\text{E}$, $9.8^\circ\text{S} - 45.5^\circ\text{N}$) known as Asia mercator region.

2.5 Statistical evaluation

The pixel of MODIS TERRA within that 8km grid cell were averaged to create one pair of MODIS TERRA and INSAT 3A CCD NDVI. This results into 1024 NDVI values of MODIS TERRA for single value of CCD. The NDVI values were randomly taken out from different natural targets like agriculture, forest, desert and snow to cover all type of land cover. The root mean square error (RMSD) and mean absolute deviation (MAD) has been computed by following formulae

$$RMSD = \sqrt{\frac{\sum_i [(P_i) - (O_i)]^2}{N}}$$

$$MAD = \frac{\sum_i ABS[(P_i) - (O_i)]}{N}$$

Where P_i = NDVI_{CCD} at i^{th} case
 O_i = NDVI_{MODIS} at i^{th} case
 N = number of paired datasets

3. RESULTS AND DISCUSSION

3.1 Effect of atmospheric correction on CCD NDVI

Atmospherically corrected NDVI has been generated by applying Rayleigh and Mie corrections using average atmospheric conditions. The corrected NDVI was then compared with atmospherically uncorrected NDVI over Indian sub-continent. It was found that for a particular clear day, the NDVI range increased from -0.2 to 0.6 in uncorrected one to -0.2 to 0.7 atmospherically corrected one. The frequency distribution of uncorrected, corrected NDVI and percent difference between them are shown in Figure 1a, 1b and 1c, respectively. Through respective difference in NDVI ranged from -25 to 455 , but majority of pixels showed positive difference between 5 to 40% .

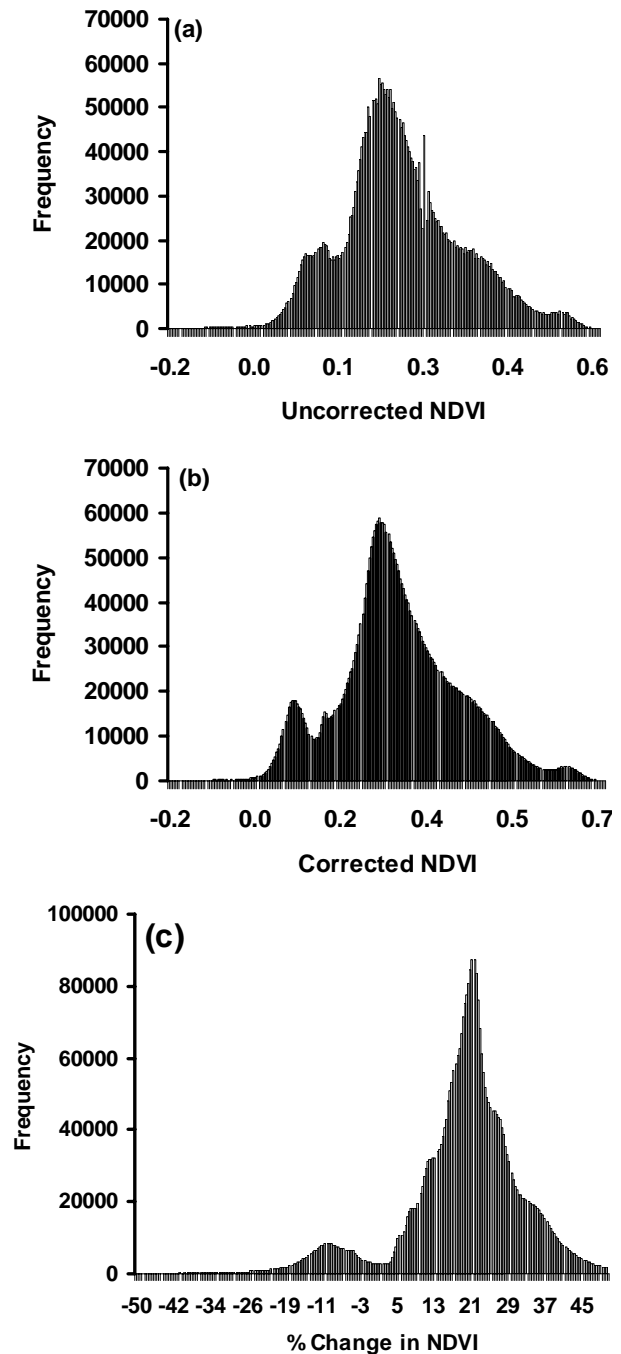


Figure 1. Comparison of Atmospherically Corrected NDVI with Uncorrected NDVI

3.2. Analysis of spatio-temporal dynamics of CCD NDVI

The 16-day NDVI composite has been computed from daily NDVI to analyze the spatio-temporal dynamics of NDVI for a growing season over different land cover categories from June 2008 to Feb 2009. In agriculture, NDVI showed quite high dynamics as compared to desert and forest, respectively. From the Figure 2, it is quite evident that in Indo-gangetic plain NDVI showed high dynamics of intensive agricultural activities. In Indo-gangetic plain,

overall spatial NDVI was low during June and but it increased from July due to increase of vegetation cover due to monsoon rainfall. The NDVI shows decreasing trend during October but shows increasing trend in November and peak in February.

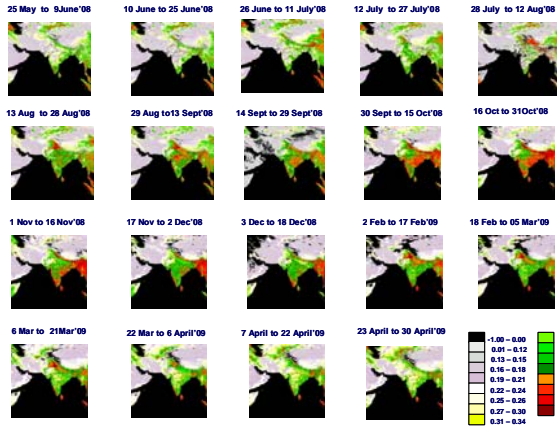


Figure 2. Spatio-Temporal Dynamics of CCD NDVI During a Growing Season

3.3 Validation

For the validation purpose, 16 day NDVI composite at 0500 GMT were used from 26th May 2008 to 30th April 2009. The 16 day composite were used to minimized the cloud interference on NDVI and to capture the phenological shift. The MODIS TERRA cloud free NDVI were available as 16 day composite at 250 m spatial resolution. These were then linearly aggregated to target CCD grid resolution. The CCD NDVI and aggregated MODIS TERRA NDVI were extracted over different land targets such as agriculture(a), forest(b) and desert(c). The temporal evolution of NDVI and rate of change of slope of the curve matches well throughout growing year with MODIS TERRA NDVI (Figure 3). Temporal profile over agricultural target in Punjab typically showed two peaks corresponding to growth of *Kharif* rice and winter wheat. In case of desert, NDVI values from both CCD and TERRA showed little change between 0.05 to 0.2 except small peak during south west monsoon period. The NDVI profiles from CCD and MODIS TERRA showed similar pattern over forest target. The spikes in the monsoon months could be due to difference in detection technology in cloud contaminated pixels. In MODIS both optical and thermal bands used for cloud screening. But only optical band data is used for cloud screening in CCD. The overall RMSD of 0.13 with a correlation of 0.83 (n=270) was obtained as shown in figure 4. The error statistics (table 1) showed higher error (0.15) in the NDVI class of 0.2 to 0.4 that corresponds to less fractional vegetative cover which could be due to higher surface anisotropy. But the errors were reduced at higher NDVI values. The error statistics were also evaluated for different land cover types as shown in table 2. Among different land cover types the maximum RMSD of 0.14 was noticed in croplands. Agriculture being the higher dynamic land cover types having prominent seasonality tends to produce more surface anisotropy surface specially during early vegetation and towards maturity stage. The presence of highly variable proportion of closed vs open canopies and determinate vs. indeterminate crops in agriculture systems are the causes of more surface anisotropy. The forest canopies are

relative more homogenous except deciduous thus resulted into less anisotropy and error. In desert also the lowest RMSD of 0.04 was noticed because the change of NDVI with time is also very low. Miura *et al.*, (2008) also reported high MODIS NDVI as compared to ASTER derived NDVI with mean difference of 0.031 from same (TERRA) platform having identical sun-target-view geometry for both the cases. In General, MODIS bands are much narrower in spectral bandwidths than ASTER red and NIR bands. Likewise, the central wavelengths from two sensors differ. MODIS red band completely avoids the red edge region (~ 680 nm), the ASTER counterpart extends to cover that wavelength. The MODIS NIR band overlaps at the longest wavelength portion of the ASTER counterpart. These are the consequences of the MODIS band selection requirements to avoid Fraunhofer lines and atmospheric absorption lines. Similarly, MODIS TERRA NDVI showed high NDVI with mean bias (NDVIMODIS – NDVICCD) of 0.07 as compared to CCD NDVI. In addition CCD NDVI computation does not explicitly consider complex modeling of surface BRDF and adjacency effects as incorporated in MODIS.

CCD NDVI class	n	RMSD	MAB
0-0.2	69	0.08	0.06
0.2-0.4	65	0.15	0.12
0.4-0.6	48	0.13	0.10
0.6-0.8	9	0.10	0.08

Table 1: Error statistics of CCD NDVI at 0500 GMT as compared to MODIS TERRA NDVI at different Classes

Land cover type	n	RMSD	MAB
Crop land	98	0.17	0.13
Forest	56	0.14	0.11
Desert	42	0.04	0.03

Table 2: Error statistics of CCD NDVI in comparison with MODIS TERRA for different land cover class

3.4 Comparison of CCD NDVI errors with results from other NDVI products

Attempts have already been made to compare available NDVI products with ground observations and with other sensors. Gallo *et al.*, (2005) compared MODIS (1km), 16 day TERRA and AQUA NDVI with NOAA-16 AVHRR (1km), 16 day NDVI for different land cover types and observed that MODIS derived NDVI always showed higher magnitude as compare to AVHRR with a RMSD of 0.05. The maximum correlation between MODIS and AVHRR was found in evergreen forest. Gitelson and Kaufman (1998) compared simulated NDVI from MODIS and AVHRR and found slightly higher NDVI from MODIS than those from AVHRR for a variety of plant chlorophyll content levels. Steven *et al.*, (2003) did intercalibration of NDVI from different sensors and found that NDVI from different sensors were strongly linearly related to each other and interconverted to a precision of 1-2%.

Geostationary meteosat second generation (MSG) SEVIRI derived cloud free daily averaged NDVI (3km) compared with resampled daily MODIS TERRA/ AQUA NDVI (250 m) by Frensholt *et al.*, (2006). They showed fairly good agreement in the dynamic range with a tendency to little higher MSG NDVI in the beginning of the

growing season (July-August) and lower towards the end (October-November). This has been attributed to seasonal variation in solar azimuth angle, which influence observations from geostationary platform as compared to those from polar orbiting platform having lesser swath. Therefore, present comparison of CCD NDVI with MODIS TERRA showed good agreement in connection with earlier finding.

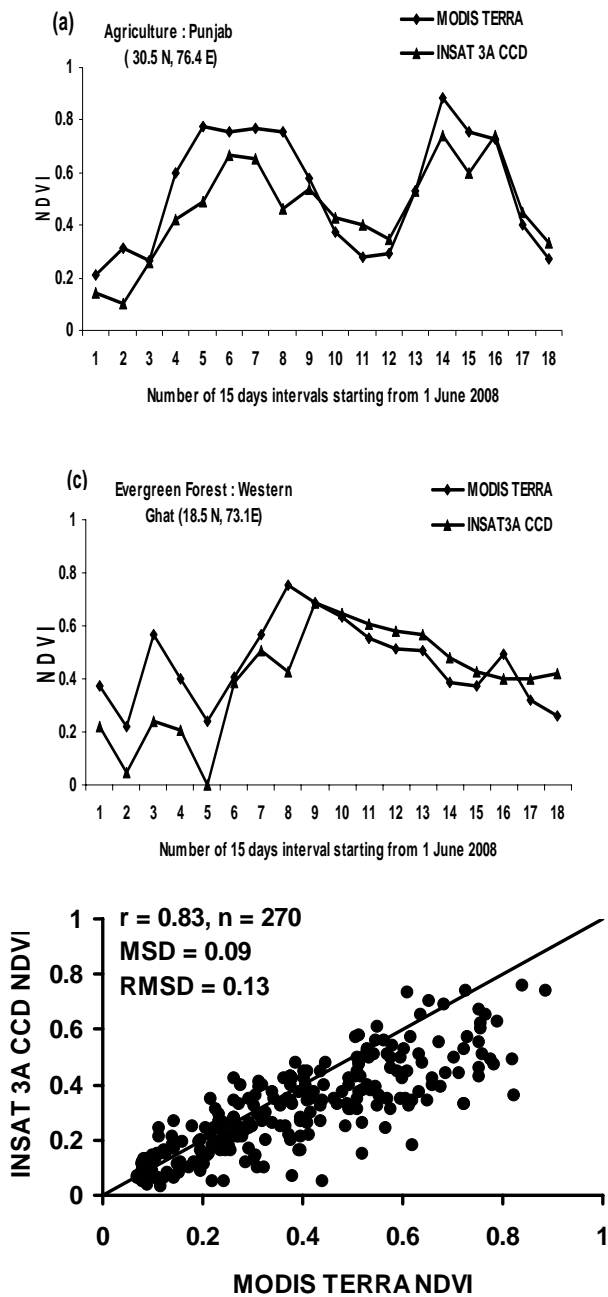


Fig. 3: Comparison of temporal profiles of CCD and TERRA NDVI over different land targets

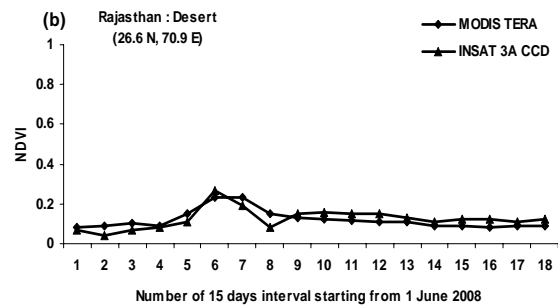


Figure 4. Comparison of INSAT 3A CCD NDVI with MODIS TERRA NDVI

CONCLUSION

A simple atmospheric correction scheme was successfully implemented to correct TOA reflectance for scattering and absorption in the atmosphere. The linear vicarious radiance calibration has been done with AWiFS for generating operational CCD NDVI. The surface reflectances in red and NIR were used to compute NDVI. The corrected NDVI was further validated with global product to judge its spatio-temporal profiles and its range over different natural targets. This study suggested that atmospheric corrected CCD temporal NDVI profile follow the same trend as globally available NDVI products in a growing region for different vegetation systems. The CCD NDVI showed fair good correlation with MODIS TERRA NDVI. The prospect appear good for future efforts to reprocess CCD data sets with a goal of continuity of NDVI product through time to study land surface changes with time. These spatial data can be used for modeling climate change studies.

ACKNOWLEDGMENTS

The authors are extremely grateful to Satellite Meteorology Division, IMD, New Delhi for providing the time series INSAT 3A CCD data from IMDPS in the purview of IMD-ISRO project. The authors would like to thank Dr. R.R. Navalgund, Director, Space Applications Centre, ISRO for his encouragement and support through out this study. The authors would also like to thank Shri. A.S. Kiran kumar, Associate Director, SAC and Dr.J.S. Parihar, Deputy Director RESA, SAC for their timely help during this study. The authors are grateful to Dr Sushma Panigrahy, Group Director, Agriculture, Forestry and Environment group for her valuable suggestions while carrying out the analysis.

REFERENCES

Asrar, G., Fuchs, M., Kanemasu, E.T., and Hatfield, J.L., 1984. Estimating absorbed photosynthetic radiation and leaf area index from spectral reflectance of wheat. *Agronomy Journal*, 76, pp. 300-306.

Bannari, A., Monin, D., and Bonn, F. 1995. A review of vegetation indices. *Remote Sensing Reviews*, 13, pp 95-120.

Bhattacharya, B. K., Nigam, R., Dorjee,N., Patel, N.K. and Panigrahy, S., Normalized difference vegetation index-towards development of operational product from INSAT 3A CCD. National Symposium ISRS, 18-20 Dec. 2008

- Fensholt, R., I. Sandholt, S. Stisen and Tucker, C., 2006. Analysing NDVI for the African continent using the geostationary meteorological second generation SEVIRI sensor. *Remote Sensing of Environment*, 101, pp. 212-229.
- Gallo, K., Lei, J., Reed, B., Eidenshink, J. and Dwyer, J., 2005. Multi-platform comparisons of MODIS and AVHRR normalized difference vegetation index data. *Remote Sensing of Environment*, 99, pp. 221-231.
- Gitelson, A. and Kaufman, Y., 1998. MODIS NDVI optimization to fit the AVHRR data series-spectral consideration. *Remote Sensing of Environment*, 66, pp. 343-350.
- Miura, T., Yoshioka, H., Fujiwara, K., and Yamamoto, H., 2008. Inter-comparison of ASTER and MODIS surface reflectance and vegetation index products for synergistic applications to natural resources monitoring. *Sensors*, 8, pp. 2480-2499.
- Rahman, H. and Dedieu, G., 1994. SMAC: A simplified method for the atmospheric correction of satellite measurements in the solar spectrum. *International Journal Remote Sensing*, 15, pp. 123-143.
- Sellers, P. J., 1985. Canopy reflectance, photosynthesis and transpiration, *International Journal Remote Sensing*, 6, pp. 1355-1372
- Spanner, M.A., Pierce, L.L., Running, S.W., and Peterson, D.L., 1990. The seasonality of AVHRR data of temperate coniferous forests: Relationship with leaf area index. *Remote Sensing of Environment*, 33, pp. 97-112.
- Steven, M. D., Malthus, T. J., Baret, F., Xu, H., and Chopping, M. J., 2003. Intercalibration of vegetation indices from different sensor systems. *Remote Sensing of Environment*, 88, pp. 412-422.
- Tucker, C.J., 1979. Red and photographic infrared linear combinations for monitoring vegetation. *Remote Sensing of Environment*, 8, pp. 127-150.
- Tucker C. J., Justice C.O. and Prince, S.D., 1986. Monitoring the grasslands of the Sahel 1984-1985. *International Journal of Remote Sensing*, pp. 1571-1571.
- Wiegand, C.L., Gausman, H.W., Cuellar, A.J., Gerbermann, A.H. and Richardsons, A.J., 1973. Vegetation density as deduced from ERTS-1 MSS response, In *Third ERTS Symposium*, NASA SP-351, US Govt. Printing Office, Washington, DC, I, pp. 93-116.
- Wiegand, C.L., Richardson, A.J. and Kanemasu, E.T., 1979. Leaf area index estimated for wheat from Landsat and their implications for evapotranspiration and crop modeling. *Agronomy Journal*, 71, pp. 336-342.
- Wiegand, C.L., Richardson, A.J., Escobar, D.E. and Gerberman, A.H., 1991. Vegetation indices in crop assessments. *Remote Sensing of Environment*, 35, pp. 105-119.